Features of structure formation in Inconel 625/WC composite coatings during laser cladding

K. O. Bazaleeva, *Candidate of Psychical-Mathematical Sciences, Leading Researcher[1], e-mail: bazaleeva-ko@rudn.ru*
D. E. Safarova, *Post-Graduate Student, Junior Research Assistant[1], e-mail: safarova_de@pfur.ru*
Yu. Yu. Ponkratova, *Researcher[1], e-mail: ponkratova-yuyu @pfur.ru*
A. V. Alekseev, *Process Engineer[1], e-mail: alexeev-anvs@rudn.ru*

[1]Peoples' Friendship University of Russia named after Patrice Lumumba, Moscow, Russia.

By varying the concentration of reinforcing phase particles and the technological parameters of the method for producing functional composite coatings, it is possible to influence their structural state and, consequently, their performance characteristics. This article analyzes the dependencies of the structural parameters of the Inconel 625/WC composite coating, manufactured by laser cladding, on the amount of reinforcing carbide phase and the cladding mode. *X*-ray phase analysis in the coatings revealed phases present in the initial powders—nickel solid solution and carbides WC and W_2C, as well as carbides formed during laser cladding: $\eta_1(Ni_3Mo_3C)$, $(W,Cr)_2C$, and $MoNbC_2$. It was established that the microhardness of the composite coating matrix primarily depends on the amount of η_1-phase in it, which increases with an increase in the initial concentration of carbide and the specific power of the laser radiation. Scanning electron microscopy and *X*-ray microspectral analysis were used to reveal the structural components and their composition. The structure includes initial spherical tungsten carbide particles containing only W and C, surrounded by a "halo" enriched with W, C, and strong carbide-forming elements of the matrix – Mo and Nb, dendrites with increased concentrations of Ni and Fe, and interdendritic space enriched with Mo, Nb, and W. It is shown that the lattice parameter of the nickel solid solution depends non-monotonically on the amount of reinforcing phase in the coating: up to 30% tungsten carbide, the lattice parameter increases with the concentration of carbide, while higher concentrations show the opposite effect.

Key words: composite metal-matrix coatings, laser cladding, phase-structural state, microhardness.
DOI: 10.17580/nfm.2025.02.02

Introduction

Advances in surface engineering technology have led to the development of various composite functional coatings that significantly increase the durability of steel parts and tools in aggressive operating conditions. Among them, coatings based on a nickel matrix reinforced with strengthening particles of ceramic phases stand out due to their excellent mechanical properties and corrosion resistance [1–3]. The use of tungsten carbide as a strengthening phase and laser cladding as a method for forming such metal matrix composite coatings is very promising [4–7].

When developing laser cladding technology for composite coatings, particular attention is paid to the influence of the amount of reinforcing phase and the technological parameters of the process that affect the thermal conditions of powder material remelting, as well as the characteristics of the structure being formed, which, in turn, determines the operational characteristics of the functional layer.

The tungsten carbide content in the composite coating significantly affects the material's microstructure and, consequently, its mechanical properties. As the WC content increases, one can expect an increase in hardness, wear resistance, and corrosion resistance [8–12]. However, potential difficulties in machinability and crack formation, which are associated with the different thermal expansion coefficients of the matrix and the strengthening ceramic phase, must be mitigated [13–16]. Therefore, to adapt coatings to specific operating conditions, it is crucial to understand the mechanisms through which tungsten carbide influences the structure and performance characteristics of the coating.

Following laser cladding, the nickel matrix predominantly exhibits a dendritic structure, which varies according to the distance of the analysed layer from the substrate, the proportion of introduced carbide, its morphology, and the technological parameters of the process [8, 17–20]. The recrystallisation conditions of the powder material change with the depth of the deposited coating, since the lower layers undergo more intense heat dissipation. Consequently, the grain structure transforms in the direction of coating growth, evolving from vertically elongated columnar crystals at the bottom to equiaxial dendrites in the middle and upper parts of the coatings. The extent of the columnar and equiaxed dendrite zones depends on

the laser cladding parameters and carbide concentration. An increase in the specific energy of laser radiation during cladding and a decrease in carbide particle concentration, which absorb the energy communicated to the composite material, lead to an increase in the zone of columnar crystals [21, 22]. Under certain laser cladding regimes and WC concentrations, the growth direction of the matrix dendrites changes: small equiaxed nickel crystals form around spherical WC particles, and columnar grains diverge from these crystals in different directions perpendicular to the WC particle surface.

During laser cladding, the strengthening carbide particles partially dissolve [23, 24]. The proportion of particles fixed in the structure is always less than that used in the synthesis of the coating. In some cases, carbide particles are completely absent from the structure. At the same time, an increase in the specific energy of laser radiation leads to greater dissolution of the carbide phase, with non-spherical particles dissolving more actively than spherical ones. However, the authors of [18] attribute the fixed proportion of carbides in the structure to the differing particles acceleration of the nickel matrix and carbide when the powder is fed into the remelting zone, and consequently to the differing probabilities of their entry into the melt bath. A certain ratio of the average diameters of the matrix and strengthening phase particles, associated with the ratio of their densities, enables an object to be formed in which the phase ratio of the initial powder is preserved.

Despite the large number of studies on the structure of composite coatings — heat-resistant nickel alloys reinforced with spherical tungsten carbide particles — their phase composition and the redistribution of elements between phases cannot be considered fully understood. The influence of carbide content and the technological parameters of the laser cladding process on these characteristics is also unclear.

Table 1
Elemental composition of Inconel 625 powde

Element	Ni	Cr	Mo	Nb	Fe	Co
C, wt. %	65.9	20.6	9.7	3.8	≤ 0.01	≤ 0.01

Table 2
Elemental composition of tungsten carbide powder

Element	W	C	Fe	Al	Cu	Cr
C, wt. %	95.8	4.0	0.2	≤ 0.01	≤ 0.01	≤ 0.01

Table 3
Marking of experimental samples

P/V, W · min/mm	Volume fraction of the carbide phase, vol.%					
	0	10	20	30	40	50
1	–	10–1	20–1	30–1	40–1	–
1.25	0–1.25	10–1.25	20–1.25	30–1.25	40–1.25	50–1.25
1.33	–	10–1.33	–	–	40–1.33	50–1.33
1.67	–	–	20–1.67	30–1.67	40–1.67	–

The aim of this study is to investigate the dependence of the structural and phase state of the Inconel 625/WC composite coating on its tungsten carbide content and on the specific energy of laser radiation. Among the structural characteristics considered in this work are the phase composition of the coating, the lattice parameter of the matrix phase, and the distribution of elements between the nickel solid solution and carbide particles.

Materials and methods

Composite coatings were formed by laser cladding on an InssTek MX-Grande machine using Inconel 625 nickel alloy and tungsten carbide powders. The powders were fed from two hoppers with control of the volume fraction of the strengthening phase.

The elemental composition of the nickel alloy powders, determined by *X*-ray fluorescence spectroscopy, and tungsten carbide is shown in **Tables 1** and **2**. The bulk density and flowability of the nickel powder were 4.56 ± 0.03 g/cm^3 and 3.40 ± 0.07 g/s, respectively, and those of the carbide powder were 10.10 ± 0.01 g/cm^3 and 8.98 ± 0.11 g/s. The powders were spherical in shape, with a matrix powder dispersion of 63–100 μm and a carbide powder dispersion of 45–106 μm.

To study the influence of the volume fraction of tungsten carbide particles on the structural and phase state of the metal matrix composite coating, samples with a carbide content of 0 to 50 vol.% were synthesized using the same cladding mode, namely, laser power P = 1000 W, beam scanning speed across the surface V = 800 mm/min. (P/V = 1.25 W·min/mm). To analyze the effect of the cladding mode on the structural characteristics of the coating, samples with the same carbide phase content but grown under different modes were prepared. In this regard, the following cladding modes were used: P = 800 W, V = 800 mm/min (P/V = 1 W · min/mm); P = 800 W, V = 600 mm/min (P/V = 1.33 W · min/mm) and P = = 1000 W, V = 600 mm/min. (P/V = 1.67 W·min/mm). The marking of experimental samples of Inconel 625/WC composite coatings is presented in **Table 3**, and the value of the P/V ratio characterizes the specific density of laser radiation during the surfacing process.

Cladding was performed on a 12X18H10T stainless steel substrate in an air atmosphere. The laser spot diameter was 1.8 mm and the distance between adjacent laser tracks was 0.7L, where L - is the width of a single track.

The phase composition of the initial powder materials and composite coatings was determined by *X*-ray diffraction using Cu-$K\alpha$ radiation. Measurements were taken with the sample rotating within the 2θ diffraction angle range of 20–100°, with a step size of 0.07° and an exposure time of 2 seconds. Quantitative phase

analysis was performed using the Diffraction Topas program, with an error margin of ±1 wt.% in determining the number of phases.

The crystal lattice parameter of the nickel γ-solid solution was determined based on the angular position of the diffraction peak (222), which did not overlap with the reflections of other phases. The peak was recorded three times with the sample repositioned, rotated at 0.02° intervals, and exposed for 4 seconds. The period determination error did not exceed ±0.0004 Å.

To determine the cause of the broadening of the diffraction maxima of the nickel solid solution, the ratio of the physical broadening of peaks (222) and (111) $\frac{\beta_{222}}{\beta_{111}}$ was evaluated [25]. The physical broadening of the peak β was determined by approximation [26] using the formula:

$$\beta = 0.5\, B\,(1 - b/B + \sqrt{1 - b/B}),$$

where B is the integral broadening of the diffraction peak, which was determined from the reflection profile using the Diffrac.Eva program with an accuracy of ±0.01 degrees; b is the geometric broadening of the diffraction peak, which can be defined as the integral broadening of the peak of the reference sample, which has no physical broadening. In this case, Inconel 625 alloy was used as a reference, obtained by laser cladding from powder and annealed at 1050 °C for 1 hour.

X-ray structural analysis was performed on samples electro-polished in an electrolyte consisting of 78 ml $HClO_4$, 730 ml C_2H_6O, 100 ml $C_6H_{14}O_2$, and 90 ml distilled water at a voltage of 10 V for 15 min.

The microstructure of the composite coatings obtained was studied using optical and scanning electron microscopy (SEM) equipped with an attachment for micro-*X*-ray spectral analysis. To reveal the structure, electrolytic etching was performed in an aqueous solution of chromic anhydride, with a mass fraction of CrO_3 of 1 ÷ 5%, at a voltage of 2.5 ÷ 5 V; the concentration of the solution and the etching mode varied depending on the concentration of carbide in the coating.

The microhardness of the coatings was also measured at a load of 200 g, with a measurement error not exceeding 15%.

Results and discussion

Fig. 1 shows the structure of composite coating 40-1, as obtained through metallographic analysis (see **Table 3**). Dark, spherical tungsten carbide particles are evenly distributed within the light nickel matrix of the coating. This coating has no cracks or large pores. Similar structures were observed in the other coatings, but cracks were found in samples 40-1.25, 40-1.33 and 50-1.25.

X-ray phase analysis of the initial Inconel 625 nickel alloy powder revealed reflections only from the FCC crystal lattice of nickel γ-solid solution. The tungsten carbide powder contained WC and W_2C carbides with a hexagonal crystal lattice, as well as free tungsten and graphite. The relative amount of W_2C carbide was twice that of the WC phase.

Fig. 2 shows the diffractograms of composite coatings with tungsten carbide content ranging from 10 to 50%, obtained by surfacing with a P/V ratio of 1.25 W · min/mm, and **Table 4** presents the results of quantitative phase analysis of these coatings. The diffraction patterns show that the structure of all composite coatings contains the initial nickel solid solution and WC and W_2C carbides. In the diffraction pattern of coating 10–1.25, in addition to the reflections from the initial phases, an additional reflection appears at a diffraction angle of 41.5 degrees.

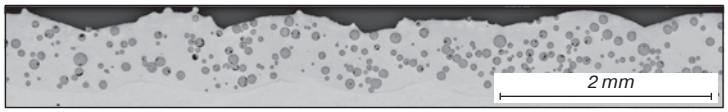

Fig. 1. Structure of composite coating with 40% tungsten carbide

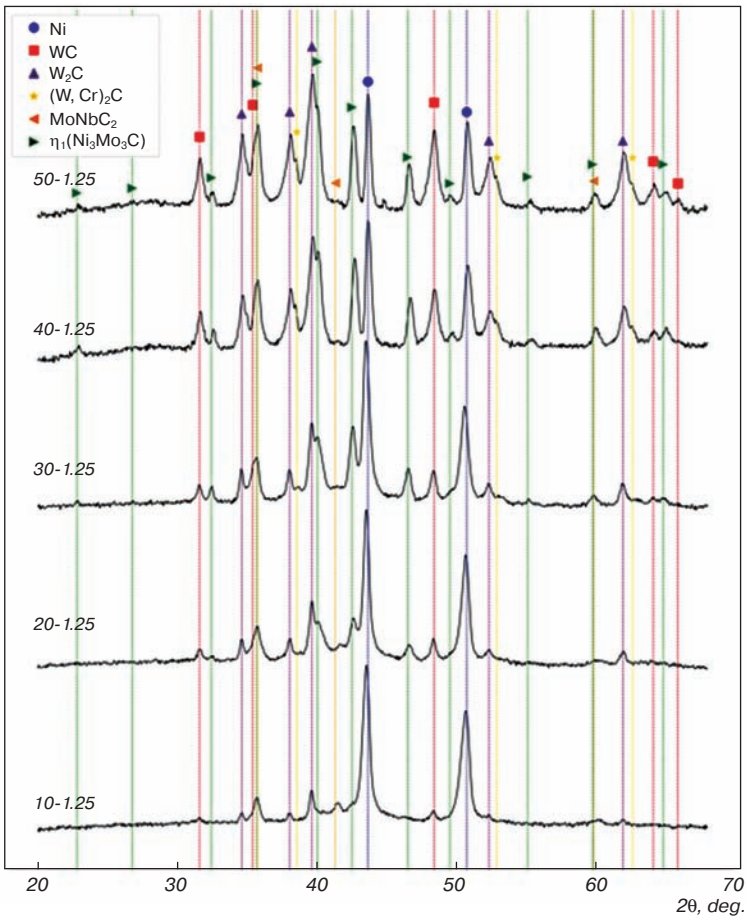

Fig. 2. Change in the diffraction pattern of the composite coating depending on the tungsten carbide content

Presumably, this reflection corresponds to the $MoNbC_2$ cubic lattice phase. Starting from a tungsten carbide concentration of 20%, when the initial carbide phases dissolve, $\eta_1(Ni_3Mo_3C)$ carbide with a cubic crystal lattice forms in the structure. On the diffractograms of coatings 40-1.25 and 50-1.25, the W_2C phase lines are split into two: presumably, this is due to the formation of a phase isomorphic to W_2C carbide in the structure, but shifted towards smaller interplanar distances; probably $(W,Cr)_2C$.

As shown in **Table 4**, an increase in the content of the strengthening carbide phase in the coating leads to an increase in the concentration of the initial WC and W_2C carbides in the structure, as well as a significant increase in the proportion of the η_1-phase synthesized during laser cladding. However, adding 40% tungsten carbide results in the amount of η_1-phase in the coating remaining almost unchanged.

Table 4

Phase composition of composite coatings depending on tungsten carbide content and claddin

Mode	Phase quantity, mass.%					
	WC	W_2C	$(W,Cr)_2C$	$\eta_1(Ni_3Mo_3C)$	$MoNbC_2$	(Ni)
10-1	1	2	–	1	2	94
10-1.25	1	2	–	2	2	93
10-1.33	1	2	–	2	2	93
20-1	2	4	–	5	2	87
20-1.25	1	3	–	7	1	88
20-1.67	1	2	–	7	1	89
30-1	2	4	1	4	1	88
30-1.25	2	4	2	18	1	73
30-1.67	2	5	–	26	1	66
40-1	4	9	2	18	1	66
40-1.25	5	12	5	27	1	50
40-1.33	5	14	3	24	1	53
40-1.67	3	8	1	39	1	48
50-1.25	9	19	8	22	1	41
50-1.33	6	14	3	36	1	40

The results of the study investigating the effect of laser cladding regime on the phase composition of composite coatings containing different amounts of hardening phase are presented in **Fig. 3** and **Table 4**. The table shows that, within the margin of error, the laser cladding regime does not change the phase composition of coatings containing 10 or 20% hardening phase. However, at higher concentrations of the strengthening phase, an increase in the specific density of laser energy (P/V ratio) results in an increase in the amount of η_1-phase in the coating and a decrease in the amount of nickel solid solution. **Fig. 3, *a*, *b*** shows the effect of specific energy density on the phase composition of coatings containing 30 and 40% tungsten carbide. In coatings containing 30% tungsten carbide, an increase in P/V leads to an increase in the relative intensity of the η_1-phase maxima and a shift towards smaller diffraction angles (i.e. larger interplanar distances), which can be explained by a change in phase composition. In contrast, an increase in the P/V ratio in coatings containing 40% tungsten carbide does not lead to a shift in the lines; only an increase in the intensity of the phase maxima is observed. Analysis of the angular position of the η_1-phase diffraction maxima for coatings with different tungsten carbide contents showed that, at a carbide

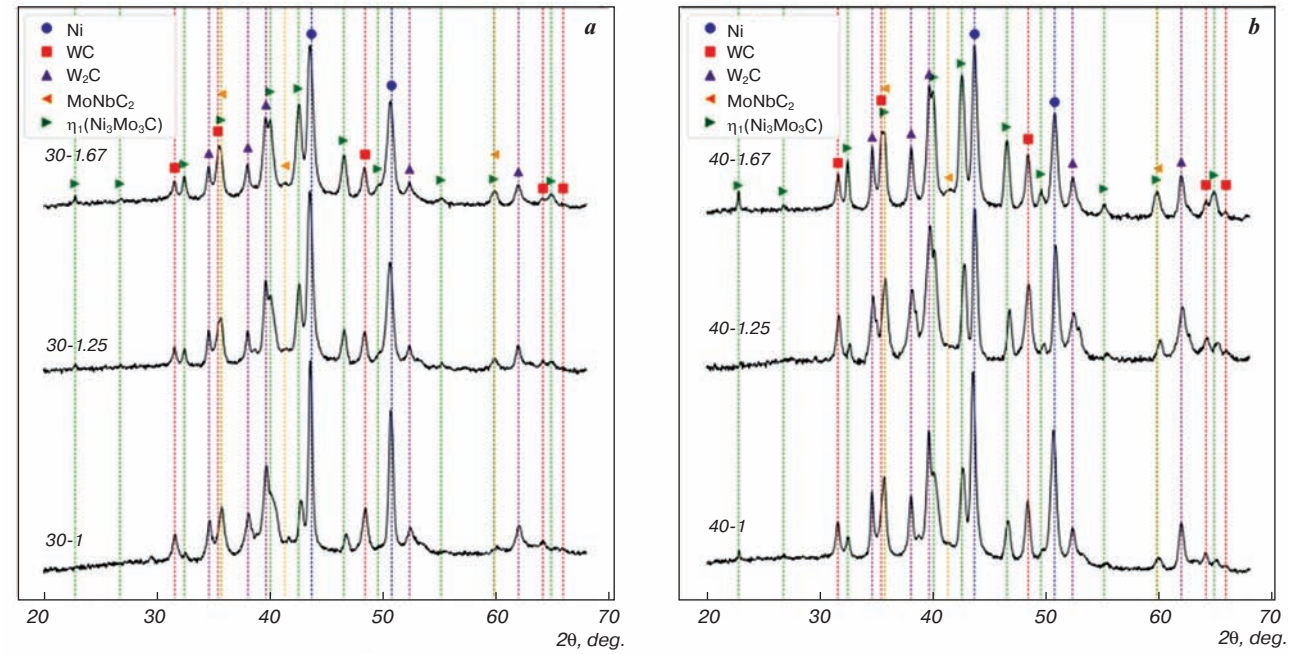

Fig. 3. Diffractograms of composite coatings with 30% (*a*) and 40% tungsten carbide (*b*)

concentration of 10–30 vol.%, an increase in the specific energy of the laser radiation leads to an increase in the η_1-phase lattice period. However, at 40–50% carbide, the η_1-phase lattice period is independent of the cladding mode.

It can be assumed that an increase in the amount of η_1-phase formed during laser cladding should be accompanied by a decrease in the content of the initial carbide phases WC and W_2C in the coating, but this effect becomes noticeable only on the diffractograms of coatings with a tungsten carbide concentration of 50%. In other coatings, the change in the amount of the initial carbide phases does not exceed the error of their determination.

The dependence of the concentration of carbide $(W,Cr)_2C$ on the specific density of laser energy is non-monotonic: the maximum amount of this phase is recorded at a ratio of $P/V = 1.25$ W·min/mm.

Fig. 4 shows structural changes in coatings depending on the amount of strengthening phase. The microstructure of the obtained composite coatings is represented by spherical particles of the initial carbide phase (zone I in **Fig. 4** (40-1.25)), a "halo" around the spherical particles (zone II), dendrites of the matrix phase (zone III), and interdendritic space (zone IV), which partly has an eutectic structure and partly consists of inclusions of excess phases. The figure shows that as the proportion of the strengthening phase increases, the amount of matrix phase in the form of dendrites decreases, and inter-dendritic precipitates occupy an increasing volume. Analysis of the elemental composition of structural components using microspectral *X*-ray analysis showed that matrix elements are practically insoluble in spherical tungsten carbide particles, while the "halo" around spherical particles contains both W and strong carbide-forming matrix elements, namely Mo and Nb, dendrites are enriched with Ni and Fe, while the interdendritic space contains an increased concentration of Mo and Nb, as well as some W. Cr is distributed almost uniformly throughout the coating matrix, but Cr compounds, probably carbides, are clearly present in the interdendritic space. This distribution of elements was observed in all coatings regardless of the hardening phase content and the cladding mode.

Determining the lattice period of the nickel solid solution provides insight into the redistribution of carbide-forming elements and carbon between the carbide phases and the solid solution. The graph showing the dependence (**Fig. 5, *a***) of the lattice period of the nickel solid solution on the initial concentration of tungsten carbide in the coating shows that an increase in the carbide content to 30% leads to an increase in the lattice period, but with a further increase in the carbide content, the opposite effect is observed – the period decreases. Presumably, the change in the lattice period is determined by two processes: the dissolution of the initial WC and W_2C carbide particles in the nickel solid solution and the precipitation of a new carbide phase η_1. The first process leads to an increase in the period, since carbon dissolves in the solid solution by the mechanism of intercalation, and tungsten atoms with a larger atomic radius dissolve by the mechanism of substitution. The formation of a new carbide phase, on the contrary, leads to a decrease in the period, since during this process carbon and large

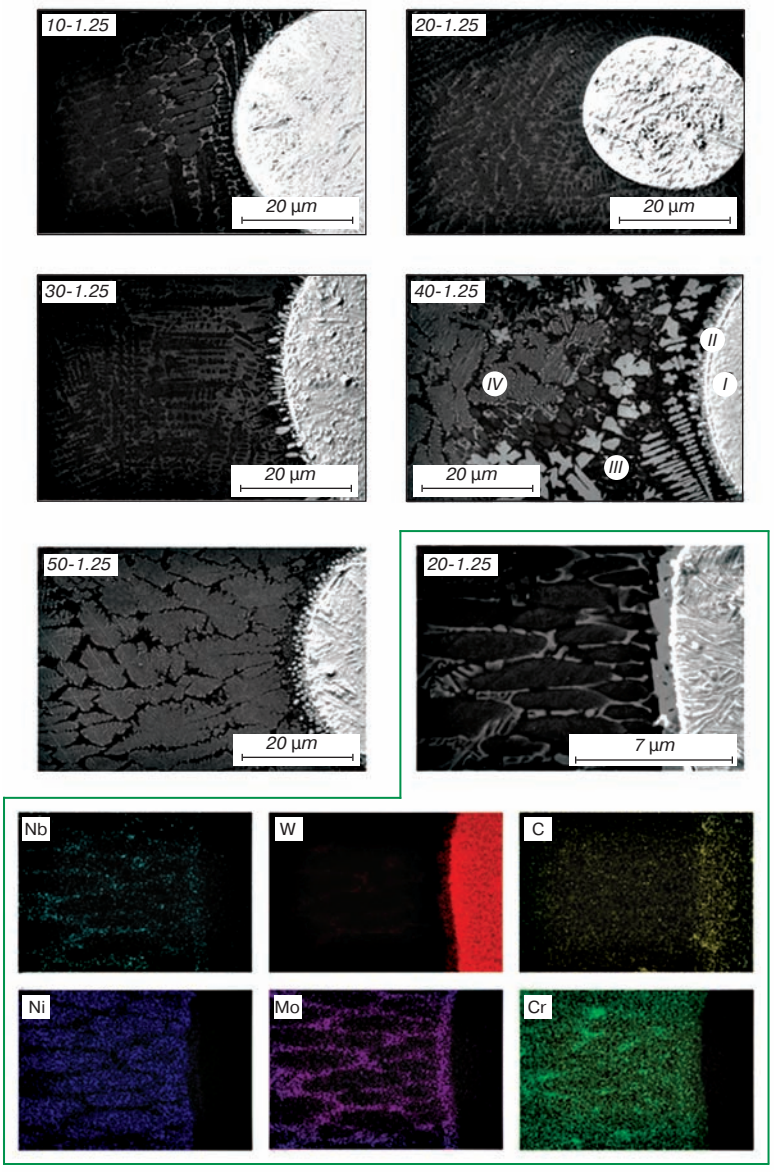

Fig. 4. Change in the structure of Inconel 625/WC composite coatings with increasing concentration of the strengthening phase (SEM) (I – initial tungsten carbide; II – "halo" around the initial carbide particles; III – nickel matrix dendrites; IV – interdendritic space) and distribution of chemical elements across the coating structure 20-1.25 (microspectral *X*-ray analysis)

atoms of carbide-forming elements leave the solid solution. It is likely that the addition of 30 vol.% carbide achieves the maximum solubility of tungsten carbide in a nickel solid solution. Thus, at a concentration of the strengthening phase in the coating of up to 30%, the dissolution of the initial carbides has a significant effect on the lattice parameter, a further increase in the carbide content leads to a predominant influence on the carbide precipitation period η_1.

When highlighting the physical broadening β of the Ni(111) and Ni(222) diffraction peaks and determining the ratio $\frac{\beta_{222}}{\beta_{111}}$, it was established that, regardless of the concentration of the strengthening carbide phase and the surfacing mode, it is close to 2.75 at $\frac{tg\vartheta_{222}}{tg\vartheta_{111}} = 2.76$, and $\frac{\sec\vartheta_{222}}{\sec\vartheta_{111}} = 1.38$, where ϑ is the diffraction angle of the maximum. It is known that the contribution to physical broadening proportional to tgϑ is caused by microdistortions of the crystal lattice, which in this case are presumably associated with the heterogeneity of the distribution of chemical elements in the γ-solid solution.

It has been shown that the dependence of the diffraction peak width on the concentration of tungsten carbide in the coating is inverse to the dependence of the lattice period (**Fig. 5, *a***): an increase in the lattice period is accompanied by a decrease in the broadening of the diffraction peak and vice versa. Probably, the most active dissolution of the initial tungsten carbides, which causes an increase in the lattice period, occurs when the matrix is in a molten state, when the atoms of the dissolved phases are relatively quickly distributed homogeneously throughout the entire volume of the coating. The separation of new carbide phases, causing a decrease in the lattice period, probably occurs in the solid state, when diffusion processes require more time, resulting in a more heterogeneous structural state formed during carbide separation.

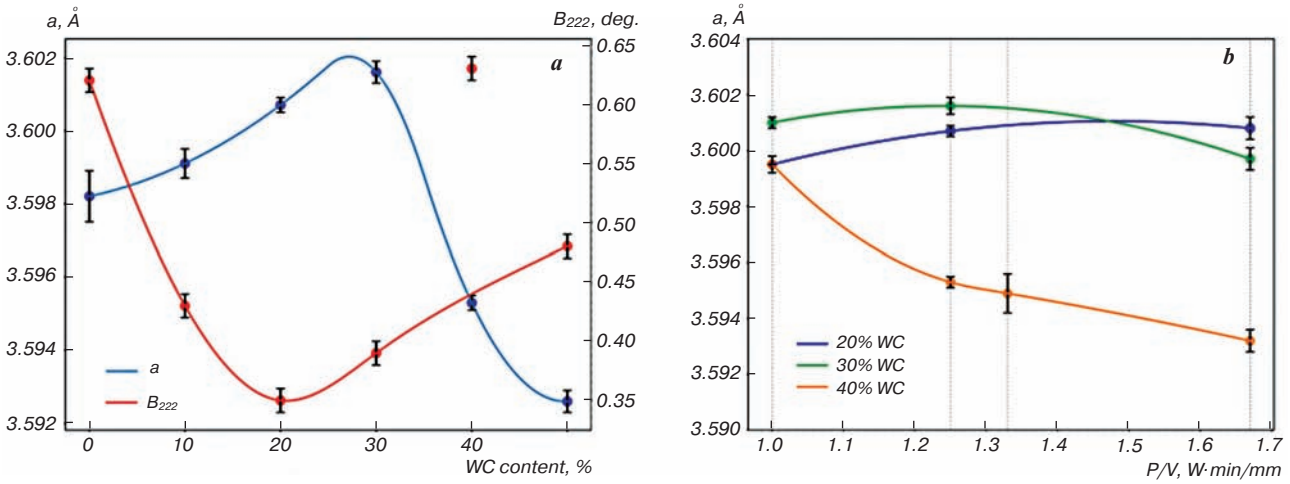

Fig. 5. Crystal lattice period γ-solid solution depending on the carbide phase content in the coating (*a*) and depending on the laser cladding regime (*b*); integral broadening of the Ni(222) diffraction maximum depending on the tungsten carbide content in the coating (*a*)

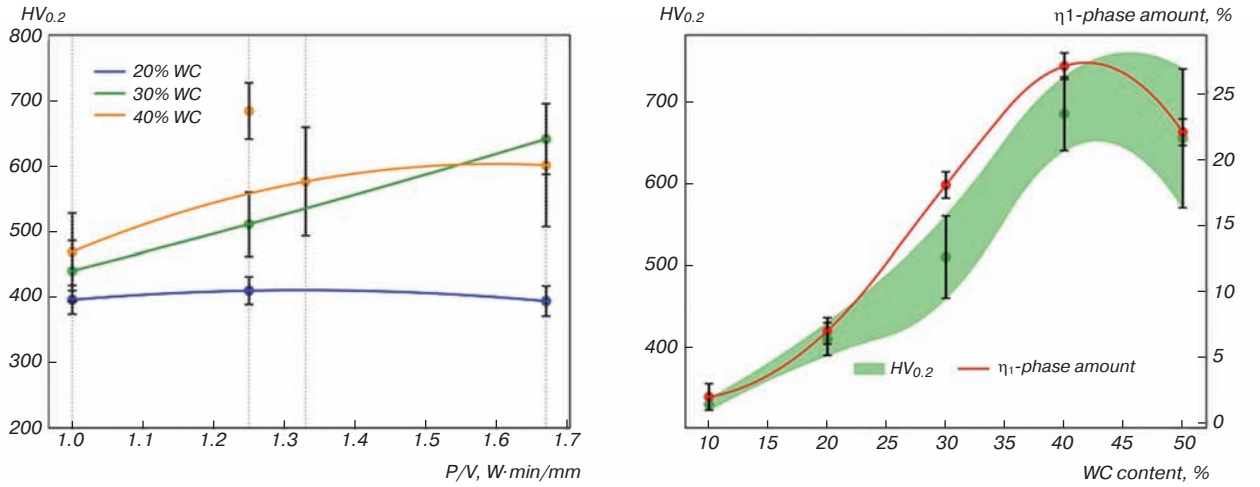

Fig. 6. Influence of tungsten carbide content in the coating (*a*) and laser cladding regime (*b*) on the microhardness of the composite coating matrix

It has been established that an increase in the specific energy density of the laser has a different effect on the crystal lattice parameter of the nickel solid solution depending on the tungsten carbide content in the coating (**Fig. 5, *b***): with an initial carbide content of 10 and 20%, an increase in energy leads to an increase in the lattice period; with an initial carbide concentration of 30%, the dependence of a (*P/V*) is non-monotonic: when the *P/V* ratio increases from 1 to 1.25 W·min/mm, the period increases, with a further increase in the specific energy density, the period decreases; at 40 and 50% tungsten carbide, an increase in energy leads to a decrease in the period. This result may be due to the fact that at 30% the maximum solubility of tungsten carbide in a solid solution is reached, and an increase in energy only leads to an increase in the amount of η_1 phase synthesized during the surfacing process, while at lower concentrations of W carbide, an increase in energy leads to additional dissolution of the initial carbide in the matrix.

It has been established that adding more than 20 vol.% of tungsten carbide to the coating leads to a gradual increase in the microhardness of the matrix, while adding 40–50% of the strengthening phase increases the hardness of the matrix relative to Inconel 625 by almost two times (**Fig. 6, *a***). For coatings containing more than 20% tungsten carbide, an increase in the specific power of the laser also leads to an increase in hardness (**Fig. 6, *b***). Analysing the influence of dispersion and solid solution strengthening mechanisms on the alloy based on changes in the phase composition and lattice period of the γ-solid solution, it can be concluded that the hardness of the alloy correlates with the amount of η_1 (Ni_3Mo_3C) synthesized during cladding (**Fig. 6, *a***). A significant increase in the error of microhardness measurement of the matrix with an increase in the concentration of the initial carbide in the coating is associated with a transition to a more heterogeneous state, caused, as mentioned above, by the uneven distribution of carbide phases throughout the matrix structure.

Conclusions

A structural analysis was performed on Inconel 625/WC composite coatings synthesized by laser cladding using different carbide phase concentrations and process conditions.

X-ray phase analysis showed that the coating structure contains a Ni-based γ-solid solution, the initial carbide phases WC and W_2C, as well as the carbides η_1 (Ni_3Mo_3C) and $MoNbC_2$ synthesized during laser cladding. With a tungsten carbide content of 40 and 50% in the coating, reflections from $(W,Cr)_2C$ carbide were additionally recorded.

Quantitative phase analysis has established that an increase in the tungsten carbide content in the coating and an increase in the specific power of the laser radiation cause an increase in the proportion of the η_1 (Ni_3Mo_3C) phase in the structure.

It has been shown that in coatings with a tungsten carbide content of less than 30%, an increase in carbide content, as well as an increase in the specific power of laser energy, leads to an increase in the crystal lattice period of the γ–solid solution, while for coatings with a tungsten carbide content of more than 30%, the opposite effect is observed: an increase in carbide content and specific laser energy power reduces the γ-solid solution period. Presumably, this difference in the behavior of solid solution coatings with different hardening phase contents is explained by the fact that at 30% tungsten carbide, its maximum solubility in the γ-solid solution is reached.

Analysis of the Ni(222) and Ni(111) diffraction peak profiles revealed that the physical broadening of the peaks is associated with microdeformation of the γ-solid solution crystal lattice, which is presumably explained by the heterogeneity of the distribution of chemical elements in the phase. It was found that the broadening of the diffraction maxima increases with a decrease in the lattice period.

Using scanning electron microscopy, the initial spherical tungsten carbides and a "halo" around the tungsten carbides, consisting of W, Mo, Nb, and C. The coating matrix had a dendritic structure, with the central part of the dendrites enriched with Ni and the interdendritic space enriched with Mo, Nb, and W.

It has been established that the greatest influence on the microhardness of the coating matrix is exerted by the amount of carbide η_1 (Ni_3Mo_3C) in the structure: the higher the content of η_1-phase, the greater the hardness.

This publication was produced as part of research project No. 202516-2-000, Grant Support Systems for Scientific Projects of PFUR.

R. B. Shipsev, E. V. Bazaleev, M. D. Savelyev, and D. Z. Ishmukhametov also contributed to this work.

References

1. Muvvala G., Karmakar D. P., Nath A. K. In-Process Detection of Microstructural Changes in Laser Cladding of In-Situ Inconel 718/TiC Metal Matrix Composite Coating. *Journal of Alloys and Compounds*. 2018. Vol. 740. pp. 545–558.

2. Chen L., Zhao Y., Meng F., Yu T., Ma Z., Qu S., Sun Z. Effect of TiC Content on the Microstructure and Wear Performance of In Situ Synthesized Ni-Based Composite Coatings by Laser Direct Energy Deposition. *Surface and Coatings Technology*. 2022. Vol. 444. 128678.

3. Soboleva N. N., Nikolaeva E. P., Makarov A. V., Malygina I. Yu. The Influence of Chromium Carbide Additive on the Structure and Abrasive Wear Resistance of the NiCrBSi Coating Formed by Laser Cladding. *Frontier Materials & Technologies*. 2020. №. 1. pp. 68–76.

4. Karmuhilan M., Kumanan S. A Review on Additive Manufacturing Processes of Inconel 625. *Journal of Materials Engineering and Performance*. 2022. Vol. 31 pp. 2583–2592.

5. Huebner J., Kusiński J., Rutkowski P., Kata D. Microstructural and Mechanical Study of Inconel 625–Tungsten Carbide Composite Coatings Obtained by Powder Laser Cladding. *Archives of Metallurgy and Materials*. 2017. Vol. 62, Iss. 2. pp. 531–538.

6. Zafar F., Emadinia O., Conceição J., Vieira M., Reis A. A Review on Direct Laser Deposition of Inconel 625 and Inconel 625-Based Composites—Challenges and Prospects. *Metals*. 2023. Vol. 13, Iss. 4. pp. 787–812.

7. He S., Park S., Shim D. S., Yao C., Li M., Wang S. Effect of Substrate Preheating on the Microstructure and Bending Behavior of WC-Inconel 718 Composite Coating Synthesized via Laser Directed Energy Deposition. *International Journal of Refractory Metals and Hard Materials*. 2023. Vol. 115. 106299.

8. Tian Z. H., Zhao Y. T., Jiang Y. J., Ren H. P. Microstructure and Properties of Inconel 625+ WC Composite Coatings Prepared by Laser Cladding. *Rare Metals*. 2021. Vol. 40. pp. 2281–2291.

9. Li H., Hu Y., Di R., Yuan R., Shi C., Lei J. Effects of WC Particles on Microstructure and Mechanical Properties of 316L Steel Obtained by Laser Melting Deposition. *Ceramics International*. 2022. Vol. 48, Iss. 14. pp. 20388–20399.

10. Huebner J., Kata D., Rutkowski P., Petrzak P., Kusiński J. Grain-Boundary Interaction Between Inconel 625 and WC During Laser Metal Deposition. *Materials*. 2018. Vol. 11, Iss. 10. 1797.

11. Zhang K., Ju H., Xing F., Wang W., Li Q., Yu X., Liu W. Microstructure and Properties of Composite Coatings by Laser Cladding Inconel 625 and Reinforced WC Particles on Non-Magnetic Steel. *Optics & Laser Technology*. 2023. Vol. 163. 109321.

12. Buyakova S. P., Kayurov K. N., Barannikova S. A. Inhomogeneity of Deformation of Surfaced Stainless Steel. *Izvestiya Vuzov. Chernaya Metallurgiya*. 2024. Vol. 67, Iss. 6. pp. 679–685.

13. Shen X. He X., Gao L., Su G., Xu C., Xu N. Study on Crack Behavior of Laser Cladding Ceramic-Metal Composite Coating with High Content of WC. *Ceramics International*. 2022. Vol. 48, Iss. 12. pp. 17460–17470.

14. Sadhu A., Choudhary A., Sarkar S., Nair A. M., Nayak P., Pawar S. D., Nath A. K. A Study on the Influence of Substrate pre-Heating on Mitigation of Cracks in Direct Metal Laser Deposition of NiCrSiBC-60% WC Ceramic Coating on Inconel 718. *Surface and Coatings Technology*. 2020. Vol. 389. 125646.

15. Zhang H., Gu D., Ma C., Guo M., Yang J., Zhang H., Chen H., Li C., Svynarenko K., Kosiba K. Understanding tensile and creep properties of WC reinforced nickel-based composites fabricated by selective laser melting. *Materials Science and Engineering: A*. 2021. Vol. 802. 140431.

16. Afanasieva L. E., Sakharov K. A. Powder Laser Cladding of a Wear-Resistant Composite Coating. *Vestnik of Tver State Technical University. Series "Technical Science"*. 2024. Iss. 1. pp. 21–26.

17. Aleksandrova A. A., Bazaleeva K. O., Brykov A. A., Grigor'yants A. G., Balakirev E. V. Direct Laser Growth of Inconel 625/TiC Composite: Effect of Structural State of Initial Powder. *Physics of Metals and Metallography*. 2019. Vol. 120, Iss. 5. pp. 459–464.

18. He S., Park S., Shim D. S., Yao C., Zhang W. J. Study on Microstructure and Abrasive Behaviors of Inconel 718-WC Composite Coating Fabricated by Laser Directed Energy Deposition. *Journal of Materials Research and Technology*. 2022. Vol. 21. pp. 2926–2946.

19. Li W., Di R., Yuan R., Song H., Lei J. Microstructure, Wear Resistance and Electrochemical Properties of Spherical/Non-Spherical WC Reinforced Inconel 625 Superalloy by Laser Melting Deposition. *Journal of Manufacturing Processes*. 2022. Vol. 74. pp. 413–422.

20. Biryukov V. P. Optimization of Laser Surfacing Technology and Its Effect on Coating *Properties*. *Photonics Russia*. 2023. Vol. 17, Iss. 6. pp. 442–453.

21. Kruth J. P. Wang X., Laoui T., Froyen, L. Lasers and Materials in Selective Laser Sintering. *Assembly Automation*. 2003. Vol. 23, Iss. 4. pp. 357–371.

22. Wang X. C., Laoui T., Bonse J., Kruth J. P., Lauwers B., Froyen L. Direct Selective Laser Sintering of Hard Metal Powders: Experimental Study and Simulation. *The International Journal of Advanced Manufacturing Technology*. 2002. Vol. 19. pp. 351–357.

23. Rong T., Gu D. Formation of Novel Graded Interface and Its Function on Mechanical Properties of WC_{1-x} Reinforced Inconel 718 Composites Processed by Selective Laser Melting. *Journal of Alloys and Compounds*. 2016. Vol. 680. pp. 333–342.

24. Weng Z., Wang A., Wu X., Wang Y., Yang Z. Wear Resistance of Diode Laser-Clad Ni/WC Composite Coatings at Different Temperatures. *Surface and Coatings Technology*. 2016. Vol. 304. pp. 283–292.

25. Gorelik S. S., Rastorguev L. N., Skakov Yu. A. *X*-ray and Electronographic Analysis of Metals. Moscow: Metallurgiya, 1963. 296 p.

26. Krivoglaz, M. A. Theory of *X*-Ray and Thermal Neutron Scattering by Real Crystals. Moscow: Nauka, 1967. 336 p. NFM